Deep morphological network-based artifact suppression for limited-angle tomography

Ishak Ayad[1], Cécilia Tarpau[1,2,3] Mai K. Nguyen[1], and Ngoc Son Vu[1]

[1] Equipes Traitement de l'Information et Systèmes, UMR 8051, CY Cergy Paris Université, ENSEA, CNRS,Cergy-Pontoise, France
[2] Laboratoire de Physique Théorique et Modélisation, UMR 8089, CY Cergy Paris Université, CNRS Cergy-Pontoise, France
[3] Laboratoire de Mathématiques de Versailles, UMR 8100, Université de Versailles Saint Quentin, CNRS, Versailles, France

Abstract. Computed tomography has been widely used in biomedical and industrial applications. The well-known filtered back-projection algorithm, probably the most used reconstruction technique, fails when the angular range used for data acquisition is not sufficient. As a consequence, reconstructions exhibit artifacts. In order to eliminate these artifacts, we propose in this article a new deep learning approach based on a U-net architecture which includes a morphological operation. This operation of mathematical morphology allows us to capture better some non-linear properties of the object to reconstruct. The proposed method provides good results for angular ranges of 170, 150, 130 and even 110 degrees. To the best of our knowledge, it is the first time a limited-angle artifact suppression method works with 110 projections.

Keywords: Computed tomography, Image reconstruction, Limited angular projections, Mathematical morphology, Deep learning, U-Net

1 Introduction

Computed tomography (CT) is one of the main imaging techniques used today in many areas such as the clinical diagnosis and material analysis. This imaging technique rests on the measurement of transmitting rays along straight lines. After being emitted by an x-ray tube, radiation is passing through the object to scan and is finally received by a detector. Such a system needs to rotate around the object to acquire a complete set of data, the data acquisition process is mathematically modelled by the classical Radon transform on lines introduced by Radon [1]. For image reconstruction, we need the inversion formula. Cormack [2] was the forerunner of CT image reconstruction with the proposition of an inversion formula for the Radon transform. This formula is the basis of the well-known filtered back-projection (FBP) algorithm. As with all analytical methods, the need for a high and uniform sampling rate is necessary. Consequently, the FBP algorithm requires complete data with an uniform sampling, that is for instance a consecutive 180° or respectively a 180° fan angle scan with

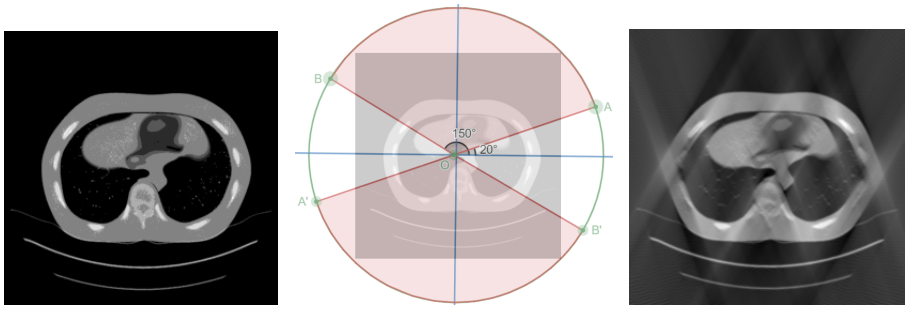

Original object X-ray tube rotation domain Reconstructed object

Fig. 1: FBP reconstruction on a Lung with $\theta \in [20°, 150°]$ and rotation step = 1 i.e. 130 projection views, The blue segments are the "distortion" artifacts due to limited-angle tomographic data, blue lines are the direction of the artifact

1° as a rotation step for parallel or fan beam reconstruction. However, when the projection data cover an angular range of less than 180°, we are faced to a limited-angle data problem. A limited-angle scan can arise in many situations, for instance where we scan a large size object, when we use large-pitch helical CT or we have to perform a restricted scanning. If one uses the FBP algorithm, this results in images with heavy directional artifacts and distortions. Some alternative reconstruction methods including optimization techniques have been studied in order to improve reconstruction quality, such as singular value decomposition (SVD) [3], total variation [4] and Tikhonov regularization [5]. Even if the obtained results may be slightly better, these techniques cannot totally correct the artifact patterns of CT images.

More recently, deep learning architectures using convolutional neural networks (CNN) have achieved overwhelming success in computer vision applications including image classification [6], denoising [7] and segmentation [8]. It is in that context that some studies proposed also to use deep learning architectures to tackle this type of image reconstruction problems. We review some of them in the next paragraph.

Gu and Ye [9] adapted the U-net architecture [8] to learn artifacts in the wavelet domain instead of directly learning the artifact-free image. Wang et al. [10] proposed a U-net-based architecture to solve the problem by pre-processing the input image using the simultaneous algebraic reconstruction technique [11] algorithm to reduce the limited-angle distortion. Tatiana and collaborators [12] proposed a framework to solve the inverse problem of limited-angle CT by combining model-based sparse regularization using shearlets with a data-driven deep neural network approach. In [13], Zhang et al. proposed an optimized deep convolutional neural network containing three layers. The objective of the first layer is to extract the feature maps. The second is a non-linear mapping which allows

reducing the artifacts, and the final layer was used to combine the extracted maps, where each layer is modeled by a convolution operation with multiple kernels. One can refer also to the work of Würfl et al. [14], where he proposed a neural network architecture based on FBP to learn the compensation weights for limited-angle reconstruction. This particular method showed some limits for small angular ranges, e.g from 120°. In [15], Wang et al. proposed a deep network for sinogram denoising and CT image reconstruction simultaneously introducing a FBP layer and combined it with two cascaded blocks.

In this paper, we concentrate on limited data coming from an incomplete angular data coverage. We give an example of such reconstruction in Fig. 1, that is, when the FBP algorithm is used to recover the object from data on a restricted angular domain of $\theta \in [20°, 150°]$. According to the considered angular range, some specific features are recovered correctly whereas other zones suffer from artifacts. This kind of artifacts is well characterized by microlocal analysis, see e.g. [16]. In fact, streak artifacts appear when the zones of the sinogram corresponding to the features of the objects were suppressed because of limited-angle data.

To remove the limited-angle artifact in CT images, we propose here a deep network based on a U-net architecture and including the opening morphological operator and residual learning. After the learning process, we faced this architecture to a validation test, different from training data, in order to prove that the model is not overfitting. The reconstruction quality is quantitatively evaluated with the peak signal noise to ratio and the structural similarity index. In addition, a comparison of our results with Tikhonov regularization and the architecture proposed by Zhang [13] is proposed.

The outline of this paper is as follows. In section 2, we present the proposed architecture suitable for artifact reduction. The obtained results are then presented in section 3. Then, Section 4 ends the paper with a discussion about the obtained results and some concluding remarks.

2 Materials and Methods

2.1 The proposition of an architecture convenient for limited-angular data problem

The proposed architecture (see Fig. 2) is a U-net with an encoder path made of 4 blocks. Each of the blocks has respectively 8, 16, 32, and 64 kernel depth and contains two successive convolutional layers with 3×3 filter with ReLu activation followed by another convolutional layer with 1×1 filter with ReLu activation and a batch normalization to avoid overfitting. A bottleneck is added with 128 filters and two convolutional layers with 3×3 filter with ReLu activation followed by another convolutional layer with 1×1 with ReLu activation. Each block consists of two operations, an extraction and a nonlinear mapping, see for instance Figure 6.

The decoder path is also made of 4 up blocks. Each block has respectively 64, 32, 16, and 8 kernel depth, and each is related to the same resolution block

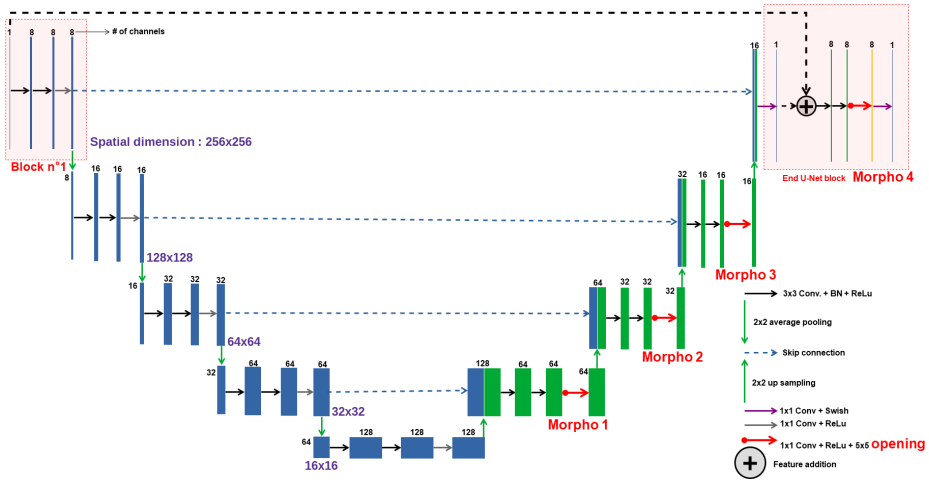

Fig. 2: Structure of the proposed deep convolutional network for artifact suppression

of the encoder via a horizontal skip connection which skips some layer in the neural network and feeds the output of one layer as the input to the next layers. A skip connection provides an alternative path for the gradient (with back propagation), and gives the localization, where each block performs the same operations as the same resolution block of the encoder. In the end block of the architecture, a skip connection between the input and the output of the U-net is also added. Thus, this allows the end block to learn the difference between the input and the output. Moreover, in order to remove noise we added, to each block of the decoder, a mathematical morphology layer which uses the opening operator (composition of erosion and dilatation [17,18]). In fact, the opening operator removes small particles (smaller than the size of the structuring element "kernel", see Figure 3 for example, where the opening operation implements the channel-wise max/min-plus convolution).

The choice of the number of filters is important, for the first block we have chosen 8 filters in order to have very few feature maps that contains artifacts (see Fig. 6). Furthermore, we can observe that using the average pooling we are able to eliminate the artifacts on 6 feature maps and that we still have one with artifacts that will be eliminated thanks to the following blocks. Then, the decoder will not only increase the resolution of the image but also correct the shape of the object thanks to the mathematical morphology layer.

2.2 Dataset

To validate our architecture for artifact reduction and compare it to existing methods, we performed an experiment on 7300 images of the standard clinical

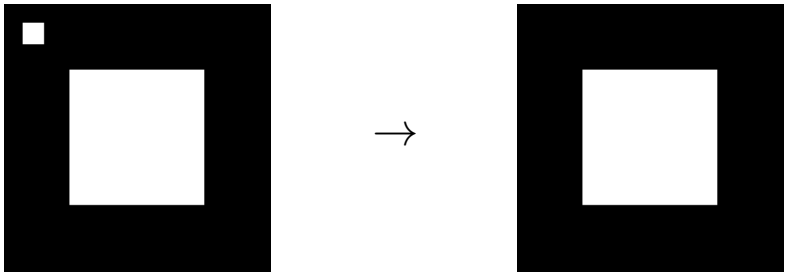

Fig. 3: (5×5) opening noise removal using the opening operator, where the noise is the small square, situated in the left-top corner of the image

dataset called PhantomFDA [19] downloaded from TCIA [20], The size of the images is 256×256 pixels. Figure 5 shows an example of used images.

Note that this dataset proposes only image reconstructions from complete set of projections. As far as the author's knowledge, no dataset providing limited angle reconstructions is available. We construct our own set of reconstructed images with different angular ranges (see Table 1) from perfect reconstructions using `radon` and `iradon` functions given in the skimage Python library [21].

Number of angular projections	Angular range
170	[10°,180°]-[0°,170°]
150	[30°,180°]-[20°,170°]
	[10°,160°]-[0°,150°]
130	[50°,180°]-[40°,170°]
	[30°,160°]-[20°,150°]
	[10°,140°]-[0°,130°]

Table 1: Angular range used to build the dataset

The input images for training and testing our algorithm (as well as the ones used to train Zhang architecture) is the FBP reconstruction.

2.3 Data augmentation

To avoid the problem of overfitting we perform some data augmentation, where 4% of the original data was taken and we have performed one of the three different transformations on each CT image randomly (see Fig. 4).

In addition to this, since the used angular range is also chosen randomly, it can be considered also as a type of data augmentation, which reinforce the robustness of the proposed reconstruction algorithm. In the proposed implementation, the probability of performing twice a reconstruction of the same image for a different angular range is 0.4.

2.4 Used libraries

We used the Tensorflow library [22] to generate our U-net architecture. This library offers us a simple manipulation of the model parameters. The global implementation of the architecture was implemented using the colab research google platform, which offers free GPU usage to accelerate the learning process.

2.5 Quantitative image analysis

To evaluate the image quality quantitatively, we used two metrics, the Peak Signal Noise to Ratio (PSNR) and the Structural Similarity Index Metric (SSIM). Denoting I_{ref} the reference image and I_{res} the resulting image of the neural network, the PNSR is obtained with the following relation

$$\text{PSNR} = 10 \times \log_{10} \left(\frac{\max(I_{\text{ref}})^2}{\text{MSE}} \right) \tag{1}$$

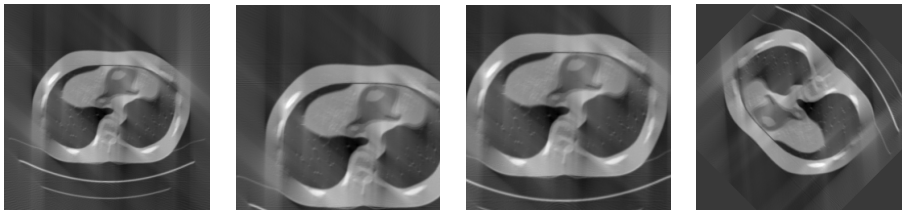

(a) (b) (c) (d)

Fig. 4: Example of obtained images by data augmentation. (b) is the result of applying a cropping with (200, 200) as a crop size, (c) a cropping followed by a translation of 25 shifted pixels and (d) results in the rotation of a random angle between 10° and 180° from the original FBP reconstructed image (a) with 130 angular projections

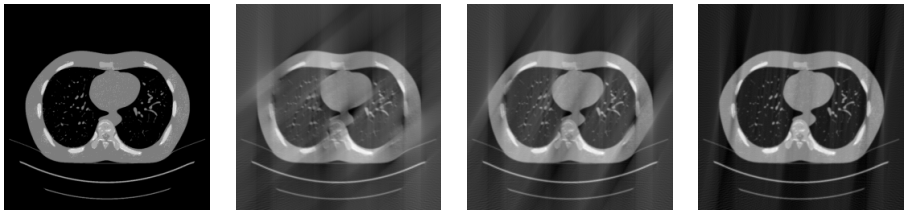

(a) (b) (c) (d)

Fig. 5: Example of used image. FBP reconstructions (b,c,d) for a respective amount of 130, 150 and 170 angular projections from the original image (a)

where the Mean Squared Error (MSE) is defined as:

$$\mathrm{MSE} = \frac{1}{N^2} \times \sum_{i=1}^{N} \sum_{j=1}^{N} [I_{\mathrm{ref}}(i,j) - I_{\mathrm{res}}(i,j)]^2 \tag{2}$$

N is the length/width of the image and $\max(I_{\mathrm{ref}})$ the maximum pixel value of the reference image.

In our case $\max(I_{\mathrm{ref}}) = 1$ because all images are values-normalized between 0 and 1, hence

$$\mathrm{PSNR} = -10 \times \log_{10}(\mathrm{MSE}) \tag{3}$$

According to the literature, a value between 30 and 40 dB defines a good quality image.

Furthermore, the SSIM is calculated as follows:

$$\mathrm{SSIM} = \frac{(2\overline{I}_{\mathrm{res}}\overline{I}_{\mathrm{ref}} + c_1)(2\mathrm{Cov}(I_{\mathrm{ref}}, I_{\mathrm{res}}) + c_2)}{(\overline{I}^2_{\mathrm{res}} + \overline{I}^2_{\mathrm{ref}} + c_1)(\sigma^2_{\mathrm{res}} + \sigma^2_{\mathrm{ref}} + c_2)} \tag{4}$$

where $\overline{I}$ is the mean value for I, σ^2 the variance, and covariance of intensities is defined as follows:

$$\mathrm{Cov}(I_{\mathrm{ref}}, I_{\mathrm{res}}) = \frac{1}{N-1} \sum_{i=1}^{N} \sum_{j=1}^{N} [I_{\mathrm{res}}(i,j) - \overline{I}_{\mathrm{res}}] \times [I_{\mathrm{ref}}(i,j) - \overline{I}_{\mathrm{ref}}]$$

$c_1 = (k_1\mathrm{L})^2, c_2 = (k_2\mathrm{L})^2$ are two variables to stabilize the division with weak denominator and L is the dynamic range of the pixel-values (typically this is $2^{\#bits\ per\ pixel} - 1$). $k_1 = 0.01$ and $k_2 = 0.03$ by default. A SSIM value closer to one indicates a higher degree of similarity between the predicted image and the reference image.

3 Results

To validate and evaluate the performance of the proposed architecture, we used test images that were not given to the architecture during the training process. Furthermore, we tested our model using an image reconstructed from only 110 projections to show that the model is not overfitting on the training data. In addition to quantitative inspection of the results, the mean PSNR and SSIM of the predicted images with respect to the angular range projections are calculated and summed up in Table [2, 3]. Reconstruction results show the superiority of the proposed method, compared to the existing ones.

Number of angular projections	Method	Input images mean PSNR	output images mean PSNR
170	Tikhonov	18.7	24
	Zhang algorithm[13]	–	30.7
	Proposed method	–	**34.5**
150	Tikhonov	15.5	23
	Zhang algorithm[13]	–	27.3
	Proposed method	–	**33.5**
130	Tikhonov	13.5	20
	Zhang algorithm[13]	–	24
	Proposed method	–	**32.2**
110	Tikhonov	10.4	18
	Zhang algorithm[13]	–	19.9
Used only for tests	Proposed method	–	**28**

Table 2: Mean PSNR value for 110, 130, 150 and 170 angular range projections. Comparison between the input and the predicted images obtained with Tikhonov regularization, the architecture proposed by [13] and the proposed method.

Number of angular projections	Method	Input images mean SSIM	output images mean SSIM
170	Tikhonov	0.42	0.43
	Zhang algorithm[13]	–	0.98
	Proposed method	–	**0.99**
150	Tikhonov	0.37	0.4
	Zhang algorithm[13]	–	0.94
	Proposed method	–	**0.97**
130	Tikhonov	0.35	0.55
	Zhang algorithm[13]	–	0.87
	Proposed method	–	**0.96**
110	Tikhonov	0.17	0.28
	Zhang algorithm[13]	–	0.74
Used only for tests	Proposed method	–	**0.81**

Table 3: Mean SSIM value for 110, 130, 150 and 170 angular range projections. Comparison between the input and the predicted images obtained with Tikhonov regularization, the architecture proposed by [13] and the proposed method.

4 Discussion and Conclusions

The deep learning framework including mathematical morphology efficiently enhances the limited-angle artifact removal with significantly fewer parameters than other methods. Testing our method on images reconstructed from 130, 150

or 170 projections gives very good results, even from 110 projections without any training on this kind of data (see figure 7).

Future work will focus on adapting our method to other kinds of CT artifacts such as those from sparse-view projections, low-dose radiation. Moreover, the study of the effectiveness of the proposed method directly on signograms (instead of the images reconstructed by FBP) will also be of interest since the cause of these different artifacts is indeed the lack of data on sinograms. The study of the robustness of such architecture on more realistic data containing Poisson noise will also be a focus for our future research.

References

1. J. Radon, "Über die Bestimmung von Funktionen durch ihre Integralwerte längs gewisser Mannigfaltigkeiten," *Akad. Wiss.*, vol. 69, pp. 262–277, 1917.
2. A. M. Cormack, "Representation of a function by its line integrals, with some radiological applications," *Journal of Applied Physics*, vol. 34, no. 9, pp. 2722–2727, 1963.
3. R. Liu, L. He, Y. Luo, and H. Yu, "Singular value decomposition-based 2D image reconstruction for computed tomography," *Journal of X-ray science and technology*, vol. 25, no. 1, p. 113—134, 2017.
4. T. Gomi and Y. Koibuchi, "Use of a Total Variation Minimization Iterative Reconstruction Algorithm to Evaluate Reduced Projections during Digital Breast Tomosynthesis," *BioMed Research International*, vol. 2018, pp. 1–14, 06 2018.
5. C. Peng, W. L. Rodi, and M. N. Toksöz, *A Tikhonov Regularization Method for Image Reconstruction.* Boston, MA: Springer US, 1993, pp. 153–164.
6. A. Krizhevsky, I. Sutskever, and G. E. Hinton, "Imagenet Classification with Deep Convolutional Neural Networks," in *Proceedings of the 25th International Conference on Neural Information Processing Systems - Volume 1*, ser. NIPS'12. Red Hook, NY, USA: Curran Associates Inc., 2012, p. 1097–1105.
7. K. Zhang, W. Zuo, Y. Chen, D. Meng, and L. Zhang, "Beyond a Gaussian denoiser: Residual learning of deep CNN for image denoising," *IEEE Transactions on Image Processing*, vol. 26, no. 7, pp. 3142–3155, 2017.
8. O. Ronneberger, P. Fischer, and T. Brox, "U-net: Convolutional Networks for Biomedical Image Segmentation," *CoRR*, vol. abs/1505.04597, 2015. [Online]. Available: http://arxiv.org/abs/1505.04597
9. J. Gu and J. C. Ye, "Multi-Scale Wavelet Domain Residual Learning for Limited-Angle CT Reconstruction," *arXiv preprint arXiv:1703.01382*, vol. abs/1703.01382, 2017. [Online]. Available: https://arxiv.org/abs/1703.01382
10. J. Wang, J. Liang, J. Cheng, Y. Guo, and L. Zeng, "Deep learning based image reconstruction algorithm for limited-angle translational computed tomography," *PLOS ONE*, vol. 15, no. 1, pp. 1–20, 01 2020. [Online]. Available: https://doi.org/10.1371/journal.pone.0226963
11. A. Andersen and A. Kak, "Simultaneous Algebraic Reconstruction Technique (SART): A Superior Implementation of the ART Algorithm," *Ultrasonic imaging*, vol. 6, pp. 81–94, 02 1984.
12. T. A. Bubba, G. Kutyniok, M. Lassas, M. März, W. Samek, S. Siltanen, and V. Srinivasan, "Learning The Invisible: A hybrid deep learning-shearlet framework for limited angle computed tomography," *CoRR*, vol. abs/1811.04602, 2018. [Online]. Available: http://arxiv.org/abs/1811.04602

13. H. Zhang, L. Li, K. Qiao, L. Wang, B. Yan, L. Li, and G. Hu, "Image Prediction for Limited-angle Tomography via Deep Learning with Convolutional Neural Network," *arXiv preprint arXiv:1607.08707*, vol. abs/1703.01382, 2016. [Online]. Available: https://arxiv.org/abs/1607.08707
14. T. Würfl, M. Hoffmann, V. Christlein, K. Breininger, Y. Huang, M. Unberath, and A. K. Maier, "Deep learning computed tomography: Learning projection-domain weights from image domain in limited angle problems," *IEEE Transactions on Medical Imaging*, vol. 37, no. 6, pp. 1454–1463, 2018.
15. W. Wang, X.-G. Xia, C. He, Z. Ren, J. Lu, T. Wang, and B. Lei, "A deep network for sinogram and CT image reconstruction," *arXiv preprint arXiv:2001.07150*, vol. abs/2001.07150, 2020. [Online]. Available: https://arxiv.org/abs/2001.07150
16. J. Frikel and E. T. Quinto, "Characterization and reduction of artifacts in limited angle tomography," *Inverse Problems*, vol. 29, no. 12, p. 125007, nov 2013.
17. G. Franchi, A. Fehri, and A. Yao, "Deep morphological networks," *Pattern Recognition*, vol. 102, p. 107246, 2020. [Online]. Available: https://www.sciencedirect.com/science/article/pii/S0031320320300522
18. S. VELASCO-FORERO, "Morpholayers." [Online]. Available: http://www.cmm.mines-paristech.fr/~velasco/morpholayers/intro.html
19. M. Gavrielides, L. Kinnard, K. Myers, R. Zeng, and N. Petrick, "FDA phantom ct database: a resource for the assessment of lung nodule size estimation methodologies and software development," 03 2010.
20. K. Clark, B. Vendt, K. Smith, J. Freymann, J. Kirby, P. Koppel, S. Moore, S. Phillips, D. Maffitt, M. Pringle, L. Tarbox, and F. Prior, "The cancer imaging archive (tcia): Maintaining and operating a public information repository," *Journal of Digital Imaging*, vol. 26, no. 6, pp. 1045–1057, Dec 2013. [Online]. Available: https://doi.org/10.1007/s10278-013-9622-7
21. S. Van der Walt, J. L. Schönberger, J. Nunez-Iglesias, F. Boulogne, J. D. Warner, N. Yager, E. Gouillart, and T. Yu, "scikit-image: image processing in python," *PeerJ*, vol. 2, p. e453, 2014.
22. M. Abadi, A. Agarwal, P. Barham, E. Brevdo, Z. Chen, C. Citro, G. S. Corrado, A. Davis, J. Dean, M. Devin, S. Ghemawat, I. Goodfellow, A. Harp, G. Irving, M. Isard, Y. Jia, R. Jozefowicz, L. Kaiser, M. Kudlur, J. Levenberg, D. Mané, R. Monga, S. Moore, D. Murray, C. Olah, M. Schuster, J. Shlens, B. Steiner, I. Sutskever, K. Talwar, P. Tucker, V. Vanhoucke, V. Vasudevan, F. Viégas, O. Vinyals, P. Warden, M. Wattenberg, M. Wicke, Y. Yu, and X. Zheng, "TensorFlow: Large-scale machine learning on heterogeneous systems," 2015, software available from tensorflow.org. [Online]. Available: http://tensorflow.org/

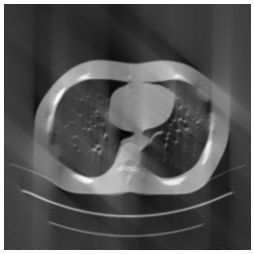

Input image from FBP reconstruction for a 130 angular projections (resolution 256×256)

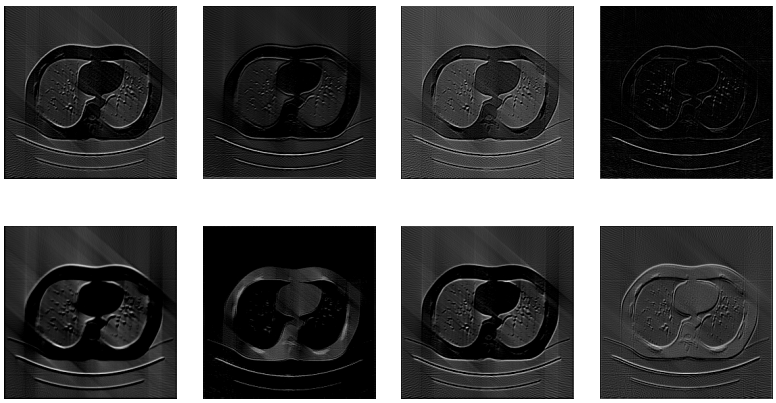

Result of the extraction block represented by two convolution operations with 8 kernels of 3×3 and ReLu activation (resolution 256×256)

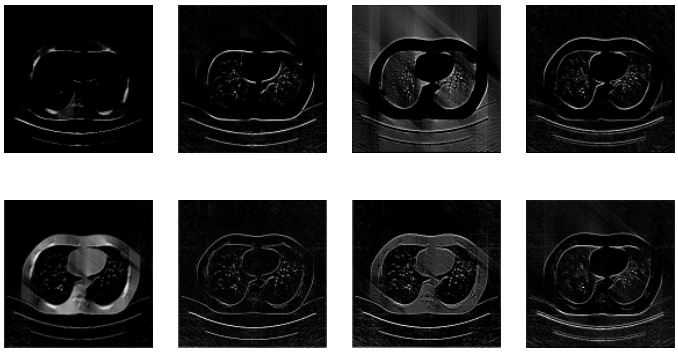

Result of the mapping block represented by one convolution operation with 8 kernels of 1×1 and ReLu activation followed by an average pooling (resolution 128×128)

Fig. 6: Result of the 1^{st} block of the proposed model

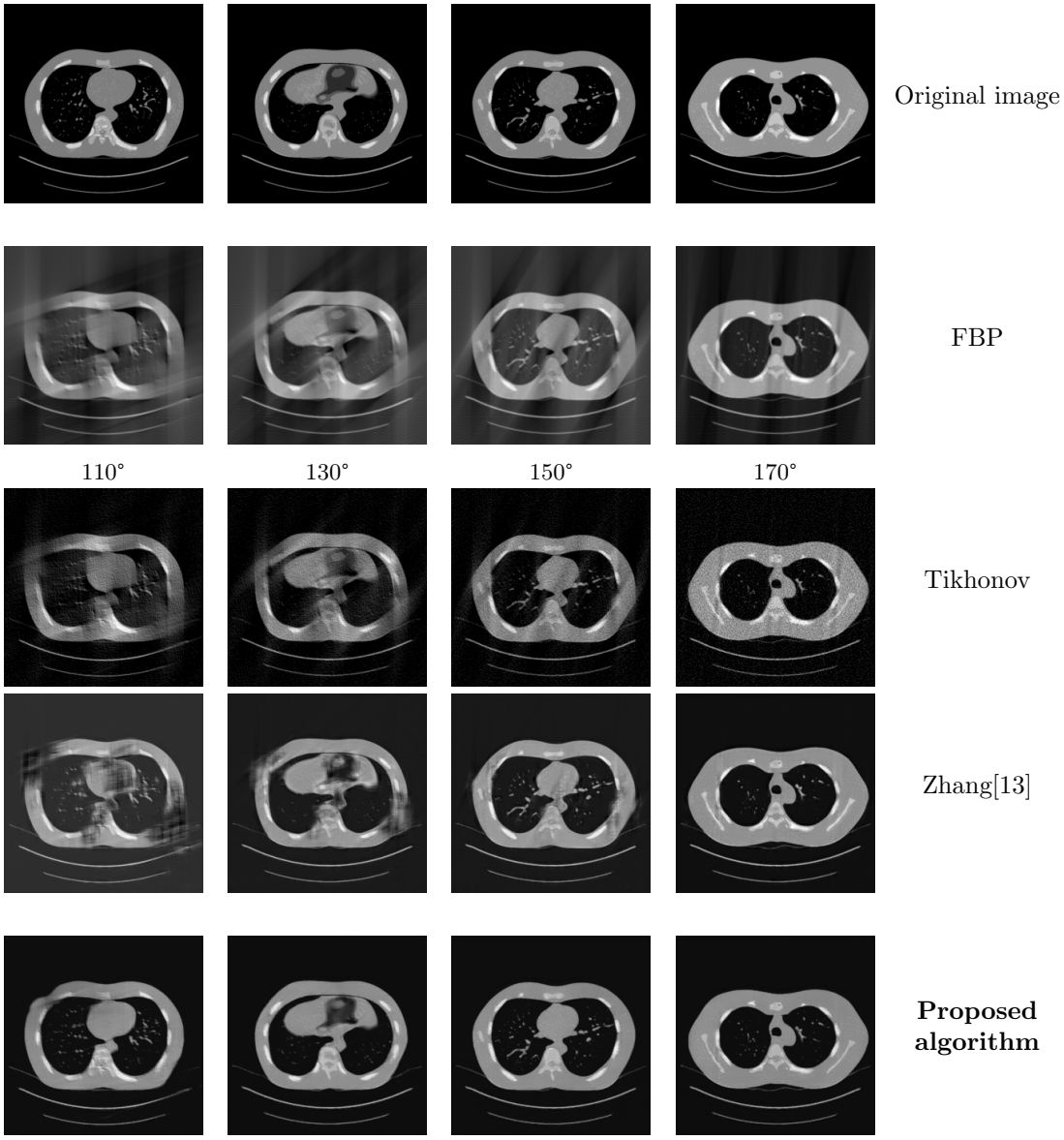

Fig. 7: Comparison of obtained results for 110, 130, 150 and 170 angular projections from original object. Using FBP reconstruction, Tikhonov regularization, Zhang algorithm and our proposed algorithm.